NANO LETTERS

Letter

Molecular-Scale Quantum Dots from Carbon Nanotube Heterojunctions

Bhupesh Chandra, Joydeep Bhattacharjee, Meninder Purewal, Young-Woo Son, Yang Wu, Mingyuan Huang, Hugen Yan, Tony F. Heinz, Philip Kim, Jeffrey B. Neaton, and James Hone

Nano Lett., **2009**, 9 (4), 1544-1548• DOI: 10.1021/nl803639h • Publication Date (Web): 11 March 2009

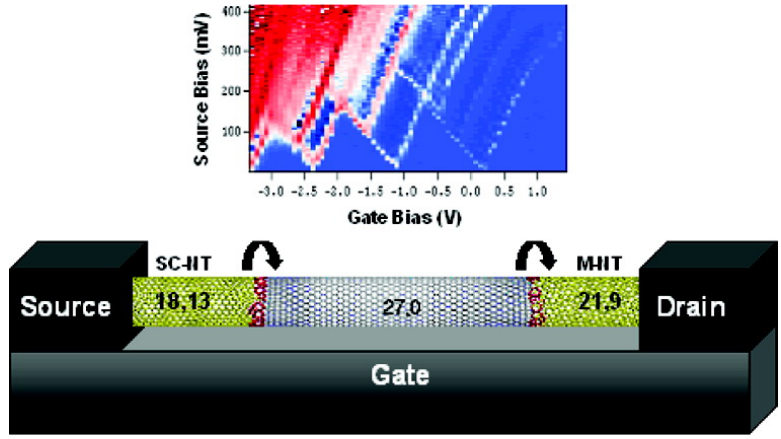

More About This Article

Additional resources and features associated with this article are available within the HTML version:

- Supporting Information
- Access to high resolution figures
- Links to articles and content related to this article
- Copyright permission to reproduce figures and/or text from this article

View the Full Text HTML

Nano Letters is published by the American Chemical Society. 1155 Sixteenth Street N.W., Washington, DC 20036

NANO LETTERS

2009
Vol. 9, No. 4
1544-1548

Molecular-Scale Quantum Dots from Carbon Nanotube Heterojunctions

Bhupesh Chandra,[†,#,¶] Joydeep Bhattacharjee,[‡,¶] Meninder Purewal,[§,#] Young-Woo Son,[||] Yang Wu,[⊥,#] Mingyuan Huang,[†,#] Hugen Yan,[⊥,#] Tony F. Heinz,[⊥,#] Philip Kim,[⊥,#] Jeffrey B. Neaton,[‡] and James Hone*[,†,#]

Department of Mechanical Engineering, Department of Applied Physics and Applied Mathematics, Department of Physics, Center for Electronic Transport in Molecular Nanostructures, Columbia University, New York, New York 10027, Molecular Foundry, Lawrence Berkeley National Laboratory, Berkeley, California 94720, and Korea Institute for Advanced Study, Seoul 130-722, Korea

Received December 2, 2008; Revised Manuscript Received February 6, 2009

ABSTRACT

Carbon nanotube heterojunctions (HJs), which seamlessly connect nanotubes of different chiral structure using a small number of atomic-scale defects, represent the ultimate scaling of electronic interfaces. Here we report the first electrical transport measurements on a HJ formed between semiconducting and metallic nanotubes of known chiralities. These measurements reveal asymmetric *IV*-characteristics and the presence of a quantum dot (QD) with ~60 meV charging energy and ~75 meV level spacing. A detailed atomistic and electronic model of the HJ enables the identification of specific defect arrangements that lead to the QD behavior consistent with the experiment.

Soon after the discovery of carbon nanotubes, it was realized that nanotubes of different chiralities can be covalently joined through the introduction of a small number of pentagon−heptagon defects, forming a nanoscale metal/semiconductor or metal/metal carbon nanotube heterojunction (HJ).[1] Despite the interest in such devices, there have been only a few direct observations of carbon nanotube HJs through scanning tunneling microscopy[2,3] and Raman spectroscopy[4,5] techniques. The only electrical transport study reported diodelike behavior across a possible metal-semiconductor HJ device,[6] identified by the presence of a sharp "kink" in the nanotube. However, no prior work has combined structural characterization and transport measurements on such HJs. Here we report detailed electrical transport measurements of a HJ connecting a (21,9) metallic nanotube and an (18,13) semiconducting nanotube, as identified by optical spectroscopy.

For this study, single-wall carbon nanotubes (SWCNTs) were grown by chemical vapor deposition across open slits (~100 μm wide) on Si/SiO_2 wafers,[7] then characterized using Rayleigh scattering spectroscopy.[8] Typically the Rayleigh spectrum remains unchanged along a suspended nanotube. The insets of Figure 1b,c show the Rayleigh spectra for the nanotube used in this study, a rare case in which the spectrum

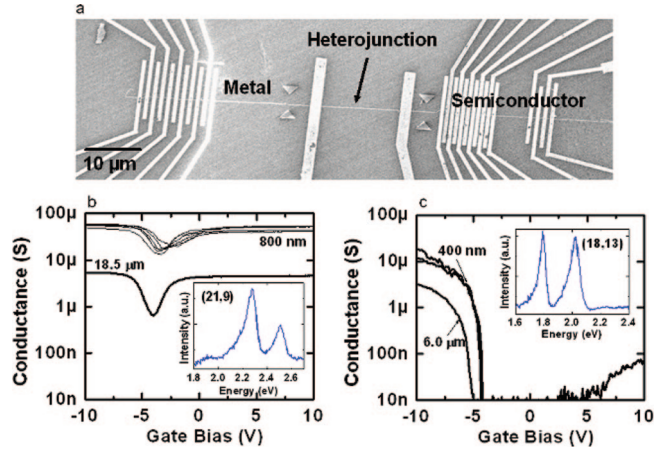

Figure 1. Device geometry and electrical measurements on semiconducting and metallic sections. (a) SEM image of the nanotube device, taken after electronic measurements. Multiple electrodes were patterned on each side of the junction to characterize the semiconducting (SC) and metallic (M) sections. A larger spacing (15.5 μm) was left for the HJ segment to allow for a possible misalignment during the tube transfer process. The arrow points toward the approximate location of the HJ. (b,c) Room-temperature Rayleigh scattering spectra (insets) and low-bias conductance vs gate voltage for the (21,9) M and (18,13) SC sections.

* To whom correspondence should be addressed. E-mail: jh2228@columbia.edu. Tel: 212-854-6244. Fax: 212-854-3304.
† Department of Mechanical Engineering, Columbia University.
‡ Lawrence Berkeley National Laboratory.
§ Department of Applied Physics and Applied Mathematics, Columbia University.
|| Korea Institute for Advanced Study.
⊥ Department of Physics, Columbia University.
Center for Electronic Transport in Molecular Nanostructures, Columbia University.
¶ These authors contributed equally to this work.

10.1021/nl803639h CCC: $40.75
Published on Web 03/11/2009

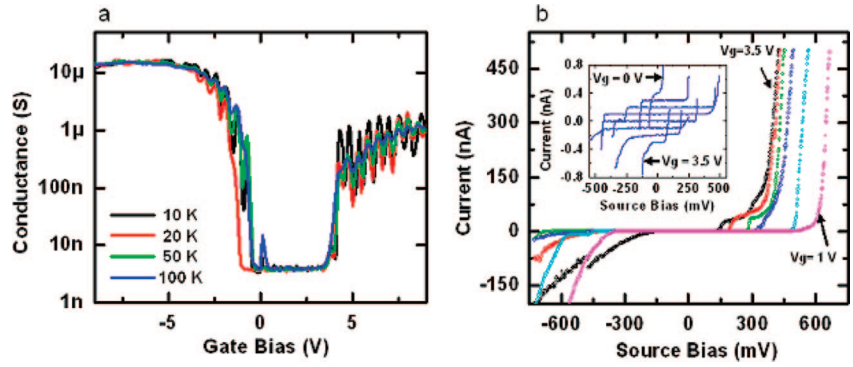

Figure 2. Temperature dependent measurements across the heterojunction. (a) Conductance gate sweep at four different temperatures, source bias is 27 mV. (b) Current−voltage measurements at 10 K for gate voltages from 1.0 to 3.5 V. The off region shifts and changes width with gate voltage, displaying a clear diamond pattern (inset, with curves offset by 0.1 nA).

changed from one typical of a semiconducting (S) SWCNT to that of a metal (M) SWCNT near the center of the suspended structure. Previous structural studies[9] allow us to assign chiral indices of (18,13) and (21,9) for the S and M sections, respectively. Because of the nanotube's mechanical integrity and because the structure change is abrupt within the size of the laser spot (∼1 μm), we conclude that the two sections are covalently joined by a linear HJ.

For electrical measurements, the suspended nanotube containing the HJ was transfer printed[10] onto a Si/SiO_2 wafer, and multiple Pd electrodes were patterned using electron-beam lithography (Figure 1a). Imaging of the central section containing the HJ by atomic force microscopy (see Supporting Information, Figure S1) revealed no visible kink and a uniform diameter of ∼2 nm, which is consistent with the assigned chiral indices.

Transport measurements on the S and M sections (Figure 1b,c) show behavior uniformly consistent with the structural assignments. All of the (21,9) devices (length 18.5 μm and 800 nm) show gate response characteristic of "chiral" metal nanotubes, which possess a small curvature-induced band-gap.[11] Analysis of the length-dependent resistance shows a low contact resistance (∼15 kΩ) and a resistivity of 9 kΩ/μm, typical for clean metallic nanotubes at room temperature.[12] The (18,13) devices (length 6.0 μm and 400 nm) likewise display behavior typical of large-diameter S nanotubes with Pd contacts.[13,14] Both chiralities show symmetric current-bias behavior.

Low-bias gate sweeps (Figure 2a) of the HJ device show ambipolar response, similar to the S sections. However, the HJ device uniquely displays strong conductance oscillations that appear below ∼100 K, and intensify at lower temperatures. Furthermore, the current−voltage behavior of the HJ (Figure 2b) is highly asymmetric, on first glimpse resembling the rectification typically seen for a M-S Schottky diode. However, the off region both shifts laterally and changes width as the gate voltage is varied, resulting in a diamond-shaped pattern as seen in the inset of Figure 2b. In addition, the $I-V$ curves show considerable structure at low temperature, in particular the presence of sharp current steps that are often succeeded by pronounced negative differential resistance. The observed conductance oscillations and current steps are inconsistent with a model of a nanotube M-S heterojunction as a simple Schottky diode and strongly suggest QD behavior. The presence of a QD is confirmed by measurement of the low-temperature (10 K) differential conductance of the HJ as a function of source and gate voltage. The resulting stability diagram (Figure 3a) shows a series of triangles of zero conductance, characteristic of the Coulomb charging spectrum of a single QD.[15,16]

In a constant interaction model[15] (Figure 3b), the stability diagram can be analyzed to yield energy scales and coupling parameters for the QD. The height of the triangles gives the electron addition energy $E_{add} \geq 135$ meV, slightly higher than the largest previously reported for a nanotube QD device.[17] The distance between the excited-state lines running parallel to the triangles gives the single-particle level spacing $\Delta E \approx 75$ meV, and the difference between E_{add} and ΔE is the Coulomb charging energy, $U \geq 60$ meV. A second indication of these two energy scales appears at larger negative gate voltages (Figure 3c), where the addition energy alternates between U and $U + \Delta E$ due to the spin degeneracy of the electronic states. The capacitances to the QD can be extracted from the stability diagram of Figure 3a by measuring the ground-state lines forming the charging diamonds with the positive and negative slopes given by $C_{gate}/(C - C_{source})$ and $-C_{gate}/C_{source}$. Here C is the sum of all the three capacitances ($C = C_{source} + C_{drain} + C_{gate}$) and is related to charging energy by $U = e^2/C$. This yields $C_{source} = 1.86$ aF, $C_{drain} = 0.46$ aF and $C_{gate} = 0.37$ aF. Finally, in a sequential tunneling model, the coupling constants of the nanotube leads to the QD can be derived from the magnitude of the current steps across an excited-state line.[18,19] At $V_g = 4$ V, the coupling of the M-SWCNT to the QD is $\gamma_m \sim 1.5-2$ meV, and the coupling between the SC-SWCNT and the QD is $\gamma_s \sim 5-12$ meV. These values remain in the 1−10 meV range at all gate voltages, while the ratio (γ_s/γ_m) varies from ∼3−6 (see Supporting Information, Figures S3 and S4).

The energy scales derived above can be used to estimate the size of the QD. In a simple picture, the level spacing is given by $\Delta E = h\upsilon_F/4L$ where υ_F is the Fermi velocity (8×10^5 m/s), h is Planck's constant, and L is the quantum confinement length. Using $\Delta E = 75$ meV, a QD length of 10 nm is obtained. The measured gate capacitance of 0.37

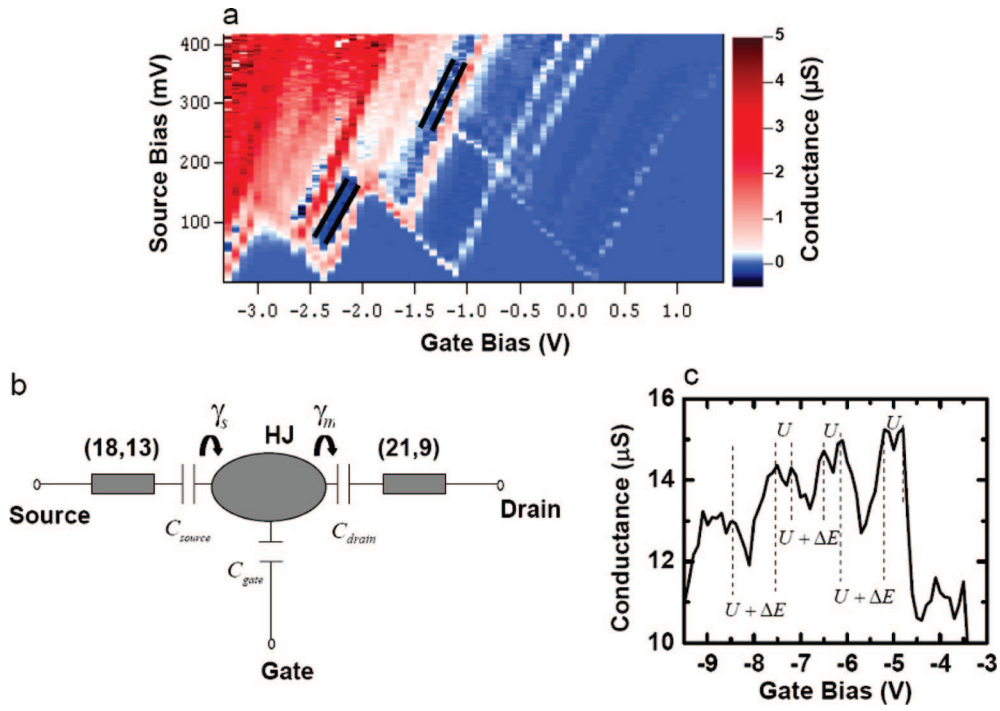

Figure 3. Transport across heterojunction. (a) Differential conductance of the HJ at $T = 10$ K, measured as a function of source-drain and gate bias for positive biases at the onset of the p-type conduction (see Supporting Information, Figure S2 for a lower-resolution plot showing both positive and negative biases). The edge of the large diamond appears near $V_g = 0.25$ V. Below this value, smaller half-diamonds with sharp edges are visible, inside which conductance is zero. Bright lines parallel to the diamond edges indicates excited states. The solid black lines next to some of the excited-state lines show regions of pronounced negative differential resistance. This is likely due to the entry of loosely coupled excited states into the bias window which then block the current through the ground-state of the QD.[34] (b) Model of the metal-semiconductor nanotube HJ device. Source, drain, and gate capacitances to the QD are denoted by C_{source}, C_{drain}, and C_{gate} respectively, γ_m and γ_s are the coupling constants of metal and semiconducting nanotube to the quantum dot. (c) Low-bias conductance vs gate voltage measurements away from the gap at $T = 10$ K. The peak separation shows a 2-fold shell filling pattern, alternating between a value corresponding to addition energy of U and one corresponding to U + ΔE.

aF yields a similar QD length of 11 nm through $C_{gate} = 2\pi\varepsilon L/[\ln(4h/d)]$, where d and L are the wire diameter and length, h (285 nm) is the gate oxide thickness and $\varepsilon = 3.9\ \varepsilon_0$ is the dielectric permittivity for thermally-grown SiO_2.

We propose that the QD is located at the HJ, based on several considerations. First, the size scale of the QD (10 nm) is much smaller than the electrode spacing (15 μm) and does not match any other physical length scale in the experiment. Second, we observe QD behavior only in the section containing the HJ and moreover have never observed this type of behavior in any single-chirality sample prepared in a similar manner. Defects such as vacancies, bond rotations, and sidewall functionalization can act as tunnel barriers,[20] and pairs of defects can produce similar QD behavior.[21,22] However, the high conductance and uniform behavior of the M and S sections, as well as the clean charging spectrum of the QD, indicate a very low density of such defects. Third, such defects typically act as resonant scatterers over a finite energy window, whereas the barriers and multiple weakly coupled electronic levels in the HJ device are evident over a wide range of gate voltages. For these reasons, it is highly unlikely that defects unrelated to the HJ are responsible for the QD behavior.

To understand what atomic-scale features might give rise to the observed behavior, we developed several detailed atomistic models of the HJ and compared their calculated electronic structure to the level spacing and coupling parameters extracted from the experiment. In principle, using just two defects, any two SWCNTs of differing chiralities can be joined[23] to form a HJ while maintaining the topological integrity of the carbon network. However, (21,9)−(18,13) HJs formed in this way introduce a bend of about 20 degrees, whereas the experiments observed a linear HJ. To construct linear interfaces, we developed a geometrical method to connect any two SWCNTs using a minimum, well-defined number of pentagon−heptagon (5−7) pair defects. We find that (18,13) and (21,9) CNTs can form topologically linear HJs using just four or nine 5−7 defects and that the HJ is most linear and also lowest in energy if the 5−7 defects are distributed uniformly along the circumference of the interface (see Supporting Information, Figure S5).

The calculated (see Supporting Information) local density of states for these HJ structures reveals localized states at the interface, much more so for nine-defect HJs (Figure 4a−c) with the degree of spatial confinement being sensitive to their arrangement. However, these new interface states are strongly resonant to the electronic states in the (21,9) nanotube and broadened considerably compared with their energy spacing in contrast to the experimental observation that $\gamma_{m,s} \ll \Delta E$ (see Supporting Information, Figure S6). Evidently QDs cannot be formed from HJs consisting of a single interface.

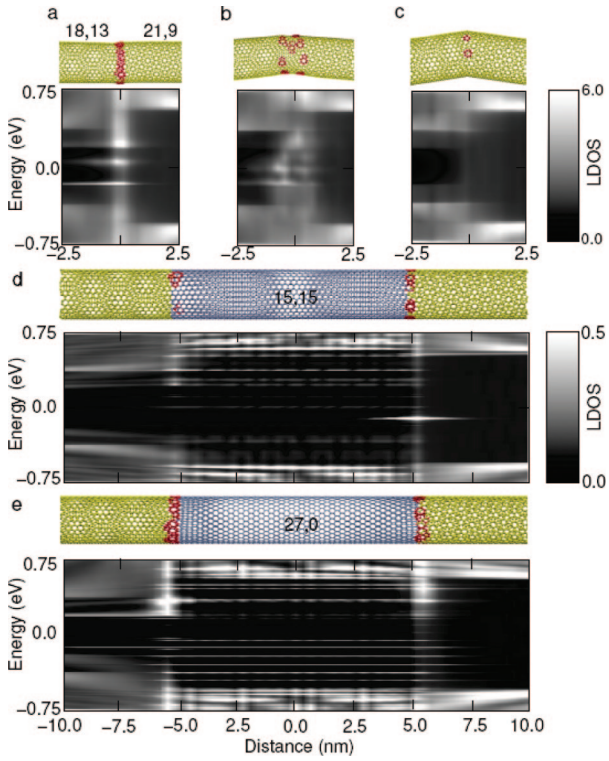

Figure 4. Calculated local density of states for different geometries. Spatially resolved local density of states (LDOS), averaged over rings 0.5 A wide, plotted as a function of energy along the nanotube axis for HJs with (a) a ring of nine 5−7 defects uniformly distributed over the entire circumference; (b) the nine 5−7 defects nonuniformly distributed over a HJ interfacial section 1 nm wide; and (c) a single pentagon and heptagon at the interface. White suggests a high LDOS. The Fermi level E_F is at zero. The gap of the (18,13) CNT is evident from the dark regions on the left that bracket E_F; the (21,9) tube is metallic with a finite LDOS everywhere on the right with its small curvature-induced gap neglected within the tight-binding approximation. As can be seen in panel a, a junction with uniform circumferential defect distribution results in three localized states with spacing of about 200 meV and level broadening on the order of 10 meV. Absence of LDOS peaks in panel c reflects our finding that several 5−7 defects are required to localize electronic states at the interface. (d,e) Similar LDOS contour plots are shown for the (18,13)−(15,15)−(21,9) and (18,13)−(27,0)−21,9) double heterojunctions (DHJs), respectively. States confined within the 10 nm (15,15) and (27,0) interior SWCNT segments exhibit level broadenings of about 1 meV, which is in agreement with experiment and significantly less than the level spacing, and the LDOS between two successive states is also zero. The "ladder" of states confined within the 10 nm (27,0) SWCNT is due to the two interfaces on either side of the dot which are almost entirely covered by 5−7 defects.

A tube segment of a third chirality introduced between the (18,13) and (21,9) nanotubes could naturally confine electronic states at the HJ. In fact, we find that the atomistic model that best explains the experiment is a composite HJ consisting of a roughly 10 nm long metallic tube between (18,13) and (21,9) SWCNTs. This composite interface can arise from a nine-defect HJ if some of the nine 5−7 defects migrate (see Supporting Information, Figure S7) toward (21,9) and the rest toward (18,13). Previous simulations at high temperatures indicate that Stone−Wales defects can dissociate into two 5−7 defects migrating in opposite directions,[24] resulting in a new chirality between them; calculations have also predicted[25] spatial electronic confinement and sharp resonances by separating two 5−7 defects in a carbon nanotube of a single chirality. Composite HJ structures have also previously been observed with scanning tunneling microscopy.[26]

The only metallic chiralities that can link (18,13) and (21,9) without introducing more than nine defects are (15,15), (18,12), and (17,14). Introduction of a (15,15) segment results in several new confined states with relatively uniform spacing and weak electronic coupling ($\gamma_m + \gamma_s \approx 1-10$ meV) to itinerant states in the (21,9) tube, which is in good agreement with experiment (Figure 4d, also see Supporting Information, Figure S8). However, allowing more 5−7 defects (at the expense of increasing the interface formation energy) can lead to additional possibilities for intermediate metallic chiralities. Among such possibilities, a (27,0) segment allows the maximum possible number of 5−7 defects at the two interfaces covering the entire circumference. As is shown in Figure 4e (also see Supporting Information, Figure S9), the (27,0) intermediate chirality greatly enhances the degree of spatial confinement and level spacing uniformity over the (15,15) case and provides the best explanation for the experimental data with predicted level spacing of ∼100 meV and electronic coupling ∼1 meV. More generally, we can conclude that in order to form good molecular scale quantum dots from carbon nanotube HJs, a short segment of intermediate metallic chirality is necessary and that both interfaces should be maximally linear to ensure enough 5−7 defects at each interface to cover the entire circumference.

The existence of the QD explains the ambipolar rectification behavior of the HJ device, which leads to the large asymmetric central diamond in the stability diagram (Figure 2b, inset). The height (in bias voltage) of the diamond (∼600 meV) is consistent with the sum of the S band gap (predicted to be 410 meV for an (18,13) SWCNT[27]) and the QD addition energy E_{add} for first hole addition (∼190 meV), both of which must be overcome to permit conduction through the device. The rectification is a natural result of asymmetric contacts to the semiconducting tube.[28,29] At the Pd contact, pinning of s-NT bands results in a voltage-tunable barrier through which electrons (or holes) must tunnel.[30] At the other S-NT contact, the existence of the HJ-QD implies that the bands of the S-NT and the QD are decoupled, so that there is no (or at least much smaller) barrier due to band bending at the S-NT-HJ interface. Finally, at gate voltages outside the central diamond, the Fermi level is outside the semiconducting gap, so the S-NT acts as a simple metallic contact to the QD. In this region, the large density of states near the semiconducting band edge explains the observed stronger coupling of the S-NT to the QD. Our result demonstrates the potential of atomically defined interfaces between carbon nanotubes as model systems for molecular scale electronic devices.[31,32] It also opens up the possibility of creating robust, room temperature single electron transistors through controlled CVD growth of nanotube HJs.[33]

Acknowledgment. We thank Mark Hybertsen and Marc Bockrath for valuable discussions. We also thank Sami Rosenblatt, Matthew Sfeir, and Christophe Voisin for as-

sistance in AFM and Rayleigh spectroscopy. We acknowledge support from the National Science Foundation under award CHE-0117752 and from Intel Corporation. Work at the Molecular Foundry was supported by the Office of Science, Office of Basic Energy Sciences, of the U.S. Department of Energy under Contract No. DE-AC02-05CH11231. Computational resources required for this work were partially provided by NERSC. We also acknowledge the Network for Computational Nanotechnology (NCN) for support.

Supporting Information Available: Material contains atomic force microscope image of the device, stability diagram across heterojunction showing complete charging diamonds, equations and analysis for extracting coupling constants, and details of the theoretical modeling framework. This material is available free of charge via the Internet at http://pubs.acs.org.

References

(1) Chico, L.; Crespi, V. H.; Benedict, L. X.; Louie, S. G.; Cohen, M. L. *Phys. Rev. Lett.* **1996**, *76* (6), 971–974.
(2) Kim, H.; Lee, J.; Kahng, S. J.; Son, Y. W.; Lee, S. B.; Lee, C. K.; Ihm, J.; Kuk, Y. *Phys. Rev. Lett.* **2003**, *90* (21), 216107.
(3) Ouyang, M.; Huang, J. L.; Cheung, C. L.; Lieber, C. M. *Science* **2001**, *291* (5501), 97–100.
(4) Anderson, N.; Hartschuh, A.; Novotny, L. *Nano Lett.* **2007**, *7* (3), 577–582.
(5) Doorn, S. K.; O'Connell, M. J.; Zheng, L. X.; Zhu, Y. T.; Huang, S. M.; Liu, J. *Phys. Rev. Lett.* **2005**, *94* (1), 016802.
(6) Yao, Z.; Postma, H. W. C.; Balents, L.; Dekker, C. *Nature* **1999**, *402* (6759), 273–276.
(7) Huang, L. M.; Cui, X.; White, B.; O'Brien, S. P. *J. Phys. Chem. B* **2004**, *108*, 16451.
(8) Sfeir, M. Y.; Wang, F.; Huang, L. M.; Chuang, C. C.; Hone, J.; O'Brien, S. P.; Heinz, T. F.; Brus, L. E. *Science* **2004**, *306* (5701), 1540–1543.
(9) Sfeir, M. Y.; Beetz, T.; Wang, F.; Huang, L. M.; Huang, X. M. H.; Huang, M. Y.; Hone, J.; O'Brien, S.; Misewich, J. A.; Heinz, T. F.; Wu, L. J.; Zhu, Y. M.; Brus, L. E. *Science* **2006**, *312* (5773), 554–556.
(10) Huang, X. M. H.; Caldwell, R.; Huang, L. M.; Jun, S. C.; Huang, M. Y.; Sfeir, M. Y.; O'Brien, S. P.; Hone, J. *Nano Lett.* **2005**, *5* (7), 1515–1518.
(11) Ouyang, M.; Huang, J. L.; Cheung, C. L.; Lieber, C. M. *Science* **2001**, *292* (5517), 702–705.
(12) Purewal, M. S.; Hong, B. H.; Ravi, A.; Chandra, B.; Hone, J.; Kim, P. *Phys. Rev. Lett.* **2007**, *98* (18), 186808.
(13) Chen, Z. H.; Appenzeller, J.; Knoch, J.; Lin, Y. M.; Avouris, P. *Nano Lett.* **2005**, *5* (7), 1497–1502.
(14) Javey, A.; Guo, J.; Wang, Q.; Lundstrom, M.; Dai, H. *Nature* **2003**, *424* (6949), 654–657.
(15) Kouwenhoven, L. P.; Austing, D. G.; Tarucha, S. *Rep. Prog. Phys.* **2001**, *64*, 701–736.
(16) Beenakker, C. W. J. *Phys. Rev. B* **1991**, *44* (4), 1646–1656.
(17) Postma, H. W. C.; de Jonge, M.; Yao, Z.; Dekker, C. *Phys. Rev. B* **2000**, *62* (16), 10653–10656.
(18) Deshmukh, M. M.; Bonet, E.; Pasupathy, A. N.; Ralph, D. C. *Phys. Rev. B* **2002**, *65* (7), 073301.
(19) Bonet, E.; Deshmukh, M. M.; Ralph, D. C. *Phys. Rev. B* **2002**, *65* (4), 045317.
(20) Fan, Y. W.; Goldsmith, B. R.; Collins, P. G. *Nat. Mater.* **2005**, *4* (12), 906–911.
(21) Bockrath, M.; Liang, W. J.; Bozovic, D.; Hafner, J. H.; Lieber, C. M.; Tinkham, M.; Park, H. K. *Science* **2001**, *291* (5502), 283–285.
(22) Maltezopoulos, T.; Kubetzka, A.; Morgenstern, M.; Wiesendanger, R.; Lemay, S. G.; Dekker, C. *Appl. Phys. Lett.* **2003**, *83* (5), 1011–1013.
(23) Melchor, S.; Dobado, J. A. *J. Chem. Inf. Comput. Sci.* **2004**, *44* (5), 1639–1646.
(24) Nardelli, M. B.; Yakobson, B. I.; Bernholc, J. *Phys. Rev. Lett.* **1998**, *81* (21), 4656.
(25) Chico, L.; López Sancho, M. P.; Muñoz, M. C. *Phys. Rev. Lett.* **1998**, *81* (6), 1278.
(26) Ouyang, M.; Huang, J. L.; Lieber, C. M. *Acc. Chem. Res.* **2002**, *35* (12), 1018–1025.
(27) Saito, R.; Dresselhaus, G.; Dresselhaus, M. S. *Physical Properties of Carbon Nanotubes*; Imperial College Press: London, 1998.
(28) Yang, M. H.; Teo, K. B. K.; Milne, W. I.; Hasko, D. G. *Appl. Phys. Lett.* **2005**, *87* (25), 253116.
(29) Freitag, M.; Radosavljevic, M.; Zhou, Y. X.; Johnson, A. T.; Smith, W. F. *Appl. Phys. Lett.* **2001**, *79* (20), 3326–3328.
(30) Heinze, S.; Tersoff, J.; Martel, R.; Derycke, V.; Appenzeller, J.; Avouris, P. *Phys. Rev. Lett.* **2002**, *89* (10), 106801.
(31) Guo, X. F.; Small, J. P.; Klare, J. E.; Wang, Y. L.; Purewal, M. S.; Tam, I. W.; Hong, B. H.; Caldwell, R.; Huang, L. M.; O'Brien, S.; Yan, J. M.; Breslow, R.; Wind, S. J.; Hone, J.; Kim, P.; Nuckolls, C. *Science* **2006**, *311* (5759), 356–359.
(32) Guo, X. F.; Gorodetsky, A. A.; Hone, J.; Barton, J. K.; Nuckolls, C. *Nat. Nanotechnol.* **2008**, *3* (3), 163–167.
(33) Yao, Y.; Li, Q.; Zhang, J.; Liu, R.; Jiao, L.; Zhu, Y. T.; Liu, Z. *Nat. Mater.* **2007**, *6* (4), 293–296.
(34) Weis, J.; Haug, R. J.; Klitzing, K. v.; Ploog, K. *Phys. Rev. Lett.* **1993**, *71* (24), 4019.

NL803639H